Ultrasensitive 2D Bi2O2Se phototransistors on silicon substrates

Fu, Qundong; Zhu, Chao; Zhao, Xiaoxu; Wang, Xingli; Chaturvedi, Apoorva; Zhu, Chao; Wang, Xiaowei; Zeng, Qingsheng; Zhou, Jiadong; Liu, Fucai; Tay, Beng Kang; Zhang, Hua; Pennycook, Stephen J.; Liu, Zheng

2019

Fu, Q., Zhu, C., Zhao, X., Wang, X., Chaturvedi, A., Zhu, C., . . ., Liu, Z. (2019). Ultrasensitive 2D Bi2O2Se phototransistors on silicon substrates. Advanced materials, 31(1), 1804945-. doi:10.1002/adma.201804945

https://hdl.handle.net/10356/139355

https://doi.org/10.1002/adma.201804945

DOI: 10.1002/
Article type: Communication

Ultrasensitive Two-dimensional Bi_2O_2Se Phototransistors on Silicon Substrates

Qundong Fu, Chao Zhu, Xiaoxu Zhao, Xingli Wang, Apoorva Chaturvedi, Chao Zhu, Xiaowei Wang, Qingsheng Zeng, Jiadong Zhou, Fucai Liu, Beng Kang Tay, Hua Zhang, Stephen Pennycook*, and Zheng Liu**

Qundong Fu, Chao Zhu, Dr. Apoorva Chaturvedi, Dr. Chao Zhu, Dr. Xiaowei Wang, Dr. Qingsheng Zeng, Dr. Jiadong Zhou, Dr. Fucai Liu, Prof. Hua Zhang, Dr. Zheng Liu
School of Materials Science and Engineering, Nanyang Technological University, Singapore 639798, Singapore
E-mail: z.liu@ntu.edu.sg.
Dr. Xiaoxu Zhao, Prof. Stephen Pennycook
National University of Singapore, Department of Materials Science and Engineering, 9 Engineering Drive 1, Singapore 117575, Singapore
E-mail: steve.pennycook@nus.edu.sg.
Dr. Xingli Wang, Dr. Zheng Liu, Prof. Beng Kang Tay
CINTRA CNRS/NTU/THALES, UMI 3288, Research Techno Plaza, Singapore 637553, Singapore
Dr. Fucai Liu
School of Optoelectronic Science and Engineering, University of Electronic Science and Technology of China, Chengdu, 610054, China.
E-mail: fucailiu@uestc.eu.cn.

Keywords: two-dimensional materials, field-effect transistors, bismuth oxyselenide, phototransistor, silicon substrate

ABSTRACT:

Two-dimensional (2D) materials have been considered as intriguing building blocks for next generation optoelectronic devices. However, their photoresponse performance still needs to be improved for practical applications. Here, ultrasensitive 2D phototransistors are reported employing chemical vapor deposition (CVD)-grown 2D Bi_2O_2Se transferred onto silicon substrates with a non-corrosive transfer method. The as-transferred Bi_2O_2Se preserved high quality in contrast to the serious quality degradation in hydrofluoric acid-assisted transfer. The phototransistors showed a responsivity of 3.5×10^4 AW^{-1}, a photoconductive gain of more than 10^4, and a time response in the order of sub-millisecond. With back gating of the silicon substrate, the dark current could be reduced to several pA. This yields an ultrahigh sensitivity with specific detectivity of 9.0×10^{13} Jones, which is one of the highest values among 2D

material photodetectors and two orders of magnitude higher than that of other CVD-grown 2D materials. The high performances of the phototransistor shown here together with the developed unique transfer technique are promising for the development of novel 2D material based optoelectronic applications, as well as integrating with state-of-the-art silicon photonic and electronic technologies.

Two dimensional (2D) materials have shown great potential for high-performance electronic devices, thanks to their dangling-bond-free surface and atomic thickness which bring merits of high carrier mobility, efficient channel current regulation and higher degree of vertical integration.[1-5] Many 2D semiconducting materials have shown outstanding phototransistor performances, such as MoS_2,[6-8] WSe_2,[9, 10] GaTe[11, 12] and $SnSe_2$,[13-15] because of their suitable energy bandgap and high mobility. Recently, a new type of 2D semiconductor Bi_2O_2Se has been prepared by chemical vapor deposition (CVD) with a large area on the fluorine mica substrate (f-mica, $KMg_3(AlSi_3O_{10})F_2$).[16-17] The merits of high mobility and superior air stability make it promising for optoelectronic applications.[18-19]

However, the high dark current and small on/off ratio limit the performances of the photodetector based on Bi_2O_2Se on f-mica substrate.[20] Although a gate configuration can be used to regulate the dark current, it is difficult to realize on f-mica substrate in the photoresponse application. As the 280 nm SiO_2/Si substrate (Si substrate) possesses inherent back gating, if Bi_2O_2Se can be transferred onto the Si substrate, not only the optoelectronic performance could be much improved, but also the applications of Bi_2O_2Se will be broadened since almost all integrated circuits are rooted in the silicon substrate. In the wet transfer of Bi_2O_2Se, hydrofluoric acid (HF) becomes the only f-mica etchant, due to the inertness of f-mica and strong electrostatic interaction between the sample and the substrate. Nevertheless, the highly corrosive HF which has the ability to penetrate tissues is hazardous to handle.[21] More

importantly, since HF is well known as one component of typical buffered oxide etchant (BOE),[22] Bi_2O_2Se will be inevitably etched by HF during the transfer process.

Here, we obtained high-quality Bi_2O_2Se on 280 nm SiO_2/Si substrate (Si substrate) and demonstrated high-performance Bi_2O_2Se based phototransistors, via developing a non-corrosive transfer method. Firstly, we synthesized high-quality Bi_2O_2Se on f-mica and verified the etching effect of HF acid during the transfer processes. Based on this, a polystyrene (PS)-assisted non-corrosive transfer method[23] was developed to transfer the Bi_2O_2Se crystal onto the Si substrate. The as-transferred Bi_2O_2Se retained a high quality and showed high phototransistor performances: (i) high photoresponsivity of 3.5×10^4 AW^{-1}; (ii) high photoconductive gain of 8×10^4; (iii) fast response timescale of 0.308 ms for the rise and 0.448 ms for the decay times and (iv) high specific detectivity of 9.0×10^{13} Jones. Moreover, by applying a negative gate voltage, the dark current can be lowered to the order of pA, which is four orders of magnitude less than the value at zero gate voltage.[20]

As depicted in **Figure 1**a, layered Bi_2O_2Se belongs to the I4/mmm space group, where oxygen atoms form a tetragonal lattice and the upper and lower bismuth atoms are stacked at different sets of tetragonal interstitial sites, forming a $[Bi_2O_2]^{2+}$ layer. Meanwhile selenium atoms which are filled in the other set of sites bind the upper and lower $[Bi_2O_2]^{2+}$ layers with weak electrostatic force, giving an interlayer spacing of about 0.61 Å. Large-area single crystalline Bi_2O_2Se samples were prepared via a low-pressure chemical vapor deposition method (Figure 1b).[17] Briefly, in a 2-inch quartz tube, bismuth selenide and bismuth oxide powders were placed in the high-temperature zone while the f-mica was put at the downstream low-temperature zone. Under a pressure of 400 Torr, the growth temperature was elevated to 620 °C in 25 min and held for 40 min, and then cooled down to room temperature naturally.

As shown in Figure 1c, Bi_2O_2Se sample up to 100 μm was obtained with a square morphology, indicating the tetragonal crystal group of Bi_2O_2Se. As determined by atomic force microscopy (AFM, Figure 1d), the surface of the as-grown sample is clean and homogeneous and the

thickness is around 5.2 nm, which corresponds to an eight-layer sample. The characteristic A_{1g} peak of Bi_2O_2Se can be found at ~159.1 cm^{-1} in the Raman spectrum (Figure 1e), which shows good consistency with the prior reports.[24-25] To further determine the atomic structure and chemical composition, annular dark-field (ADF) imaging and energy-dispersive X-ray spectroscopy (EDS) mapping were conducted on an aberration-corrected scanning transmission electron microscope (STEM) system. Figure 1f shows the ADF-STEM image of a square atom lattice while Figure 1g is the corresponding fast Fourier transform (FFT) of Figure 1f. The square arrangement of spots, (200), $(1\bar{1}0)$ and (110) in Figure 1g confirms the I4/mmm space group of Bi_2O_2Se. As shown in Figure 1h-1k, EDS element mappings demonstrate the uniform distribution of elements Bi, Se and O. All the results confirm the high quality of our CVD-grown Bi_2O_2Se.

As discussed above, the inertness of f-mica and the electrostatic interaction between the Bi_2O_2Se and f-mica make it hard to do the transfer. The normal transfer process using HF acid as the substrate etchant is schematically depicted in **Figure 2**a. Firstly, PMMA was spin-coated on the surface and Bi_2O_2Se together with the PMMA film was separated from f-mica as the substrate was etched by HF. This process will take about half an hour. After transferred to the desired substrate, PMMA was removed by acetone, leaving the uncovered Bi_2O_2Se. However, usage of the corrosive HF acid is hazardous. Besides, as HF is well known as a component of BOE, the Bi_2O_2Se will definitely be etched during the above process. To demonstrate the etching effect of HF, we tracked the etching process of Bi_2O_2Se by immersing samples in the 2% HF acid. Figure 2b shows the untreated Bi_2O_2Se flake, while Figure 2d and 2f show the same sample after the HF treatment for 30 s and 90 s, respectively. As shown in Figure 2d and 2f, a high-quality square Bi_2O_2Se was partially etched after 30 s treatment and almost fully etched after 90 s treatment. The etching effect was also verified by Raman spectra shown in Figure 2c, 2e and 2g. It turns out that the Raman signal was significantly weakened after 30 s and nearly vanished after 90 s. To elaborate this etching effect, we investigated the HF-assisted

transferred sample under aberration-corrected STEM. From Figure 2h, the nonuniform contrast in the low magnification image indicates the partial etching of this sample. In addition, nanopores found in both the low and high magnification images (Figure 2i, 2j and S1) further confirmed that Bi_2O_2Se had been etched by HF acid during the transfer process. Therefore, a non-corrosive transfer method is highly demanded to transfer Bi_2O_2Se onto other substrates.

We developed a PS-assisted transfer method (schematically presented in **Figure 3**a).[23] Briefly, PS was first spin-coated on the surface of f-mica and then baked at 80 °C for 15min. Then the PS film together with Bi_2O_2Se was peeled away from the f-mica under the assistance of DI water. The PS film was then placed on the Si substrate and baked at 70 °C for 1 h, and finally washed out by toluene, leaving the Bi_2O_2Se sample on the Si substrate. The more hydrophobic surface property together with the much stiffer film property of the PS film distinguish it with the PMMA film, which make it much easier to peel off from the f-mica substrate.[23] The superior stability of Bi_2O_2Se in DI water was demonstrated in Figure 3b-3g. As a striking contrast to the HF acid treatment, no obvious changes can be found in the optical images (Figure 3b, 3d and 3f) and Raman spectra (Figure 3c, 3e and 3g) even after a 24 h DI water treatment. Figure 3h shows the optical image of Bi_2O_2Se on Si substrate after the transfer. Scanning electron microscopy (SEM) image shows a uniform surface of the as-transferred sample (Figure 3i and S2b). Raman spectrum (Figure 3j) presents the characteristic A_{1g} peak at ~159.3 cm^{-1}, which matches well with that of the sample on f-mica. More detailed characterizations (AFM and EDS) can be found in Figure S2. All of these demonstrate the robustness of our non-corrosive transfer method.

To further evaluate the quality of the samples, two-terminal devices were fabricated based on the as-transferred Bi_2O_2Se flakes with the thickness of about 8 nm on the Si substrate to examine the electrical transport and photoresponse properties. Details of the device fabrication processes are described in the method part. Figure 3k shows the output and transfer curves of the Bi_2O_2Se transistor using SiO_2/Si as a back gate. It can be seen that the transistor exhibits an

n-type semiconducting behavior, which is in accordance with previous reports.[18, 19] The two-terminal field-effect mobility (μ_{2p}) of the device could be calculated by fitting the linear region in I_d-V_g curve using the equation $\mu_{2p} = \frac{dI_d}{dV_g} \times \frac{L}{WC_iV_d}$, where L is the channel length, W is the channel width, C_i is the capacitance between the channel and the back gate per unit area ($C_i = \varepsilon_0\varepsilon_r/d$; ε_0 is vacuum permittivity, ε_r is the relative permittivity, and d is the thickness of SiO_2 layer). The μ_{2p} of the as-transferred Bi_2O_2Se device is calculated as about 107 $cm^2V^{-1}s^{-1}$, which is the same order as the reported value in a Hall mobility measurement.[16] Suppressing the scattering from the surface by encapsulating a high-k dielectric layer may further improve the mobility.[26-28]

The high FET performance of the as-transferred Bi_2O_2Se and the convenience of the gate tunability on the Si substrate make it attractive for optoelectronic applications. The optoelectronic behavior of the Bi_2O_2Se phototransistor was systematically investigated by exploring the photocurrent at different optical powers, applied drain and gate voltages. **Figure 4**a shows the photocurrent at different drain voltages under the excitation of 532 nm light with different powers. The device (inset of Figure 4a) can generate photocurrent as high as 3.5 μA even under the illumination of an incident light power of about 0.1 nW and the bias of 500 mV. As the light power increases from 0.1 nW to 5 nW, the photocurrent increases gradually from 3.5 μA to 10.7 μA (Figure S3). The light power dependence of the photocurrent is plotted with a log-log scale (Figure 4b), where the photocurrent can be expressed by a simple power law ($I_{ph} \propto P^{0.30}$). The non-unity exponent is attributed to the complex processes including the electron-hole generation, trapping, and recombination within the semiconductor.[13] One of the most important parameters for a photodetector is the photoresponsivity (R), which is the ratio of generated photocurrent (I_{ph}) and incident optical power ($R = I_{ph}/PS$, where P is the power density and S is the effective area). Figure 4c shows the photoresponsivity acquired at different light powers. The photoresponsivity reaches up to 3.5×10^4 AW^{-1}, which is one of the highest

values of reported 2D semiconductors[13,29-34] and much higher than that of the commercial Silicon device (0.5 AW^{-1}).[35] The photoconductive gain (G) is another parameter to evaluate the performance of a phototransistor, which is defined by the equation $G = Rh\upsilon/\eta q$, where η is the external quantum efficiency (EQE), q is the electron charge, h is Planck's constant, and υ is the frequency of the incident light. Assuming η = 100%, G is estimated to be ~8.0×10^4 (Figure 4c). The charge traps by the surface-bound water on the silicon substrate (photovoltaic effect) and the band tail states near the band edge (photoconductive effect) together contribute to the high gain of the phototransistor.[36-37] Note that under strong light illumination, the recombination rate of the photocarriers will increase and thus the lifetime will decrease, which results in a slight decrease of the gain in Figure 4c.[37]

The response time is a critical factor for high-speed photodetector. Here, the response time was investigated by monitoring the change of the photocurrent while alternatively turning on and off the light illumination using a mechanical chopper (see the method part). As shown in Figure 4d, the photocurrent changes as a function of time with a good repeatability. In order to investigate the fast response of the photocurrent, the photocurrent change at the initial stage of the light illumination on and off was recorded (Figure 4e and 4f). The dynamic response of the photocurrent for the rise and decay can be expressed by $I(t) = I_{\mathrm{dark}} + Aexp(t/\tau_{rise\ or\ decay})$,[38] where A, t and τ are the scaling constant, on or off state duration time and rise or decay time constant, respectively. By fitting the photocurrent trace, the rise and decay time constants of the measured device are figured out to be about 0.308 ms and 0.448 ms, respectively, which is already a very good result for photodetectors based on 2D semiconductors.[13,29-34] By using a more sensitive measurement technique like ultrafast two-pulse photovoltage correlation measurements,[39] the response time of Bi_2O_2Se could be improved in consideration of the limitation of the current equipment.

The gate bias dependence of the photoresponse was also investigated. The silicon based back-gating configuration can be applied to the as-transferred Bi_2O_2Se device for tuning the dark

current as well as the photoresponse (**Figure 5**a). Figure 5b presents the I_d-V_g curves under dark and light illumination, in which significant photocurrent is generated when the gate voltage is changed from -50 V to 50 V. As the light intensity increases, the I_d-V_g transfer curve shifts to the left significantly, owing to the positive gate effect caused by the trapped photogenerated holes in the interface between the Bi_2O_2Se channel and Si substrate. Figure 5c shows the gate dependence of the photoresponsivity, which could be tuned from 10 to 3.6×10^4 AW^{-1} under a light power of 0.2 nW and a bias of 0.5 V. Such back-gate tunability is of great importance in phototransistors because it adds an additional dimension to engineer the photoresponsivity and photoconductive gain for the detection of light in a wide range (Figure S4). The reason for the decrease of the responsivity at high gate voltage might be ascribed to the reducing contribution of the photogating effect on the photocurrent under high electrostatic gating effect.[37] Furthermore, due to the evident n-type behavior of the sample, the device shows large dark current at zero gating (hundreds of nA), which will cause a high consumption of power at the off state. By applying a negative gate voltage, the dark current could be reduced significantly to several pA because of the higher Schottky barrier. As a result, the on/off ratio of the current between the light irradiation and dark state can reach ~ 10^7 (Figure 5d). The specific detectivity (D^*) is a parameter to evaluate the sensitivity of the photodetector, which is defined by the noise equivalent power (*NEP*) equation $NEP = (A\Delta f)^{1/2}/D^*$ where A is the effective area of the photodetector and Δf is the electrical bandwidth. When the shot noise from the dark current is the major limiting factor of D^*, D^* can be expressed as $D^* = RA^{1/2}/(2eI_{dark})^{1/2}$.[40-42] As shown in Figure 5d, D^* reaches its maximum value at a gate of -32 V where a much smaller dark current and a relatively large photocurrent contribute jointly to this result. The maximum D^* obtained here is up to 9.0×10^{13} Jones, which is much higher than that of the commercial Silicon device (~10^{12} Jones).[43] Also, it is one of the highest values among 2D material based photodetectors and two orders of magnitude higher than that of other CVD-grown 2D materials reported.[13,29-34]

To compare the photodetector performances of the as-transferred Bi_2O_2Se with other 2D semiconductors prepared by CVD and mechanical exfoliation (ME) methods, the photoresponsivity (R/V_d), specific detectivity (D^*) and dynamic response time (τ_{rise}) are summarized in **Table 1**. Here we divided the photoresponsivity by the bias voltage (V_d) to exclude the contribution of V_d on the photocurrent, assuming that the photocurrent increases linearly with V_d. It is noted that the Bi_2O_2Se photodetectors show excellent performance in the photoresponsivity and specific detectivity, both of which are among the highest values in photodetectors based on 2D semiconductors. In addition, the specific detectivity of our Bi_2O_2Se photodetectors is two orders of magnitude larger than that of other CVD-grown 2D materials, which is ascribed to the reduced dark current by the back gating of Si substrate. In terms of the dynamic response time, although CVD-grown MoS_2 and SnS_2 have better performances (0.07 ms and 0.005 ms), they are limited by their much lower photoresponsivity (less than 0.1 $AW^{-1}V^{-1}$) and specific detectivity (less than 10^{10}), which are five and four orders of magnitude smaller than our results (7.0×10^4 $AW^{-1}V^{-1}$ and 9.0×10^{13} Jones). Therefore, compared with other 2D semiconductors, the as-transferred Bi_2O_2Se showed overall high photodetector performances.

In summary, we developed a non-corrosive method to transfer Bi_2O_2Se onto Si substrate, and the Bi_2O_2Se crystal retained a high quality after the transfer. We then fabricated phototransistor devices based on the as-transferred Bi_2O_2Se on a Si substrate. The devices showed overall high performances in photodetection: high responsivity of 3.5×10^4 AW^{-1}, large photoconductive gain of 8×10^4, and fast response time of 0.308 ms for the rise and 0.448 ms for the decay processes. Benefiting from the gate tunability on Si substrate, the devices showed a very low dark current as well as high specific detectivity up to 9.0×10^{13} Jones. Such ultrasensitive photodetection is promising for the development of 2D optoelectronic devices. The developed transfer method also opens a wealth of possibilities to integrate high-quality Bi_2O_2Se with the silicon complementary metal-oxide–semiconductors technologies.

Experimental Section

CVD synthesis of Bi_2O_2Se on f-mica: The CVD process is schematically depicted in Figure 1b. In detail, the setup is a split tube furnace with interconnected control system (1-Zone, 1200°C) and we used 1200 mm long fused quartz tubes with an outside diameter (O.D.) of 50 mm. Powders of Bi_2Se_3 and Bi_2O_3 were used as precursors, placed in two alumina crucibles and Bi_2O_3 was located in the central zone while Bi_2Se_3 was located in the upstream with a distance of 8 cm. The f-mice substrate was placed downstream with a distance of 12 cm. The chamber was first pumped down to 6.0×10^{-2} Torr, and then 170 sccm (standard cubic centimeter per minute) Ar was introduced to reach a pressure of 350-400 Torr. The chamber was heated to 620 °C in 25 min and held for 40 min. After that the furnace was cooled down naturally to room temperature and the chamber was refilled with Ar gas to reach atmospheric pressure.

AFM, SEM EDS and Raman characterizations: AFM was conducted under the *Asylum Research Cypher Scanning Probe Microscope* system with a tapping mode. SEM EDS characterization was performed under the *JOEL JSM-7600F* system with an accelerating voltage of 15 kV. Raman spectra were recorded by a *Witec* Raman system equipped with 100x objective lens and a grating of 1200 lines/mm under 532 nm laser excitation.

Transfer of Bi_2O_2Se onto Cu Grid (HF) and STEM characterization: The TEM samples were prepared with a poly (methyl methacrylate) (PMMA) based transfer method. First, the f-mica substrates with the as-grown CVD samples were spin-coated with PMMA at 3,000 r.p.m. for 60 s and then baked at 150 °C for 5 min. Afterward, PMMA-coated sample was peeled off by etching away the underneath f-mica in 2% HF solution. Next, the floating PMMA film was transferred to the DI water and scooped up by a TEM grid. The TEM grid was dried at 50 °C for 30 mins, and then submerged into acetone for about 24 h to remove PMMA. Finally, the TEM grid was rinsed by isopropyl alcohol (IPA) and dried in air.

ADF-STEM imaging was carried out on an aberration-corrected JEOL ARM-200F equipped with a cold field emission gun, operating at 80 kV, and an ASCOR probe corrector. The convergent semi-angle of the probe was set at about 30 mrad. ADF-STEM images were collected using a half-angle range from about 68 to 280 mrad. A dwell time of 19 μs $pixel^{-1}$ was set for single-scan imaging. EDS mapping was conducted using the Oxford X-Max 100TLE SDD EDS system.

PS-assisted transfer of Bi_2O_2Se onto Si substrate: The as-transferred Bi_2O_2Se was prepared with a PS assisted transfer method. First, the f-mica substrate with the as-grown Bi_2O_2Se was spin-coated with PS at 3,500 r.p.m. for 60 s and then baked at 85 °C for 15 min. After the edge of f-mica was cut away, PS-coated sample was peeled off by a drop of DI water. Next, the floating PS film was transferred onto Si substrate. The Si substrate was dried at 80 °C for 1 h and then heated at 150 °C for 30 mins to improve the contact between the sample and the Si substrate. Then the Si substrate was immerged into toluene for 24 h to remove PS and then into acetone for 5h to remove organic residuals. Finally, the Si substrate was dried by floating nitrogen.

Devices fabrication and measurement: After the Bi_2O_2Se was transferred onto the Si substrate, the sample was then spin-coated with PMMA. The electrode patterns were then defined by the EBL (Nova nanoSEM 230 with digital pattern generator Nabity-NPGS). After the pattern was developed in MIBK/IPA, metal contacts (3 nm Cr/55 nm Au) were deposited by Kurt J. Lesker Nano 36 Thermal Evaporator. Electrical and photoresponse properties of the FETs were measured in the MicroXact Probe Station by Agilent B1500A Semiconductor Device Parameter Analyzer. The rise and decay time of the light response was measured by Tektronix MDO 3052 Mixed Domain Oscilloscope and Stanford Research SR540 Chopper Controller.

Supporting Information

Supporting Information is available from the Wiley Online Library or from the author.

Acknowledgements

Q. F. and C. Z. contributed equally to this work. This work was supported by the Singapore National Research Foundation under NRF award number NRF-RF2013-08, Tier 2 MOE2016-T2-2-153, MOE2015-T2-2-007, Tier 1 RG164/15, Tier 1 RG4/17.

Received: ((will be filled in by the editorial staff))
Revised: ((will be filled in by the editorial staff))
Published online: ((will be filled in by the editorial staff))

References

[1] M. Liu, X. Yin, E. Ulin-Avila, B. Geng, T. Zentgraf, L. Ju, F. Wang, X. Zhang, *Nature* **2011**, *474*, 64.
[2] B. Radisavljevic, A. Radenovic, J. Brivio, i. V. Giacometti, A. Kis, *Nat. Nanotechnol.* **2011**, *6*, 147.
[3] Q. H. Wang, K. Kalantar-Zadeh, A. Kis, J. N. Coleman, M. S. Strano, *Nat. Nanotechnol.* **2012**, *7*, 699.
[4] F. Liu, W. L. Chow, X. He, P. Hu, S. Zheng, X. Wang, J. Zhou, Q. Fu, W. Fu, P. Yu, *Adv. Funct. Mater.* **2015**, *25*, 5865.
[5] J. Zhou, J. Lin, X. Huang, Y. Zhou, Y. Chen, J. Xia, H. Wang, Y. Xie, H. Yu, J. Lei, *Nature* **2018**, *556*, 355.
[6] Z. Yin, H. Li, H. Li, L. Jiang, Y. Shi, Y. Sun, G. Lu, Q. Zhang, X. Chen, H. Zhang, *Acs Nano* **2011**, *6*, 74.
[7] O. Lopez-Sanchez, D. Lembke, M. Kayci, A. Radenovic, A. Kis, *Nat Nanotechnol.* **2013**, *8*, 497.
[8] W. Zhang, J. K. Huang, C. H. Chen, Y. H. Chang, Y. J. Cheng, L. J. Li, *Adv. Mater.* **2013**, *25*, 3456.
[9] W. Zhang, M.-H. Chiu, C.-H. Chen, W. Chen, L.-J. Li, A. T. S. Wee, *Acs Nano* **2014**, *8*, 8653.
[10] T. Wang, K. Andrews, A. Bowman, T. Hong, M. Koehler, J. Yan, D. Mandrus, Z. Zhou, Y.-Q. Xu, *Nano Lett.* **2018**, *18*, 2766.
[11] F. Liu, H. Shimotani, H. Shang, T. Kanagasekaran, V. Zólyomi, N. Drummond, V. I. Fal'ko, K. Tanigaki, *Acs Nano* **2014**, *8*, 752.
[12] Z. Wang, K. Xu, Y. Li, X. Zhan, M. Safdar, Q. Wang, F. Wang, J. He, *Acs Nano* **2014**, *8*, 4859.
[13] X. Zhou, L. Gan, W. Tian, Q. Zhang, S. Jin, H. Li, Y. Bando, D. Golberg, T. Zhai, *Adv. Mater.* **2015**, *27*, 8035.
[14] P. Perumal, R. K. Ulaganathan, R. Sankar, Y. M. Liao, T. M. Sun, M. W. Chu, F. C. Chou, Y. T. Chen, M. H. Shih, Y. F. Chen, *Adv. Funct. Mater.* **2016**, *26*, 3630.
[15] X. Zhou, Q. Zhang, L. Gan, H. Li, T. Zhai, *Adv. Funct. Mater.* **2016**, *26*, 4405.
[16] J. Wu, Y. Liu, Z. Tan, C. Tan, J. Yin, T. Li, T. Tu, H. Peng, *Adv. Mater.* **2017**, *29*, 1704060.
[17] J. Wu, C. Tan, Z. Tan, Y. Liu, J. Yin, W. Dang, M. Wang, H. Peng, *Nano Lett.* **2017**, *17*, 3021.
[18] J. Wu, H. Yuan, M. Meng, C. Chen, Y. Sun, Z. Chen, W. Dang, C. Tan, Y. Liu, J. Yin, *Nat. Nanotechnol.* **2017**, *12*, 530.
[19] J. Yin, Z. Tan, H. Hong, J. Wu, H. Yuan, Y. Liu, C. Chen, C. Tan, F. Yao, T. Li, *Nat. Commun.* **2018**, *9*, 3311.
[20] J. Li, Z. Wang, Y. Wen, J. Chu, L. Yin, R. Cheng, L. Lei, P. He, C. Jiang, L. Feng, *Adv. Funct. Mater.* **2018**, *28*, 1706437.
[21] T. G. Mayer, P. L. Gross, *Annals of emergency medicine* **1985**, *14*, 149.

[22] R. Chow, W. Lanford, W. Ke‐Ming, R. S. Rosler, *J. Appl. Phys.* **1982**, *53*, 5630.
[23] A. Gurarslan, Y. Yu, L. Su, Y. Yu, F. Suarez, S. Yao, Y. Zhu, M. Ozturk, Y. Zhang, L. Cao, *Acs Nano* **2014**, *8*, 11522.
[24] T. Cheng, C. Tan, S. Zhang, T. Tu, H. Peng, Z. Liu, *J. Phys. Chem. C* **2018**, *122*, 19970.
[25] A. L. Pereira, D. Santamaría-Pérez, J. Ruiz-Fuertes, F. J. Manjón, V. P. Cuenca-Gotor, R. Vilaplana, O. Gomis, C. Popescu, A. Munoz, P. Rodriguez-Hernandez, *J. Phys. Chem. C* **2018**, *122*, 8853.
[26] J. Schrieffer, *Phys, Rev.* **1955**, *97*, 641.
[27] C. Sah, T. Ning, L. Tschopp, *Surf. Sci*. **1972**, *32*, 561.
[28] N. P. Butch, K. Kirshenbaum, P. Syers, A. B. Sushkov, G. S. Jenkins, H. D. Drew, J. Paglione, *Phys. Rev. B* **2010**, *81*, 241301.
[29] D.-S. Tsai, K.-K. Liu, D.-H. Lien, M.-L. Tsai, C.-F. Kang, C.-A. Lin, L.-J. Li, J.-H. He, *ACS Nano* **2013**, *7*, 3905.
[30] E. Liu, M. Long, J. Zeng, W. Luo, Y. Wang, Y. Pan, W. Zhou, B. Wang, W. Hu, Z. Ni, Y. You, X. Zhang, S. Qin, Y. Shi, K. Watanabe, T. Taniguchi, H. Yuan, H. Y. Hwang, Y. Cui, F. Miao, D. Xing, *Adv. Funct. Mater.* **2016**, *26*, 1938.
[31] G. Su, V. G. Hadjiev, P. E. Loya, J. Zhang, S. Lei, S. Maharjan, P. Dong, P. M. Ajayan, J. Lou, H. Peng, *Nano Lett*. **2015**, *15*, 506.
[32] P. Hu, J. Zhang, M. Yoon, X.-F. Qiao, X. Zhang, W. Feng, P. Tan, W. Zheng, J. Liu, X. Wang, J. C. Idrobo, D. B. Geohegan, K. Xiao, *Nano Res.* **2014**, *7*, 694.
[33] R. B. Jacobs-Gedrim, M. Shanmugam, N. Jain, C. A. Durcan, M. T. Murphy, T. M. Murray, R. J. Matyi, R. L. Moore, B. Yu, *ACS Nano* **2014**, *8*, 514.
[34] S. R. Tamalampudi, Y.-Y. Lu, U. R. Kumar, R. Sankar, C.-D. Liao, B. K. Moorthy, C.-H. Cheng, F. C. Chou, Y.-T. Chen, *Nano Lett.* **2014**, 14, 2800.
[35] C. O. Kim, S. Kim, D. H. Shin, S. S. Kang, J. M. Kim, C. W. Jang, S. S. Joo, J. S. Lee, J. H. Kim, S.-H. Choi, *Nat. Commun.* **2014**, *5*, 3249.
[36] G. Konstantatos, M. Badioli, L. Gaudreau, J. Osmond, M. Bernechea, F. P. G. De Arquer, F. Gatti, F. H. Koppens, *Nat. Nanotech*. **2012**, *7*, 363.
[37] M. M. Furchi, D. K. Polyushkin, A. Pospischil, T. Mueller, *Nano Lett.* **2014**, *14*, 6165.
[38] A. Grinvald, I. Z. Steinberg, *Anal. Biochem.* **1974**, *59*, 583.
[39] H. Wang, C. Zhang, W. Chan, S. Tiwari, F. Rana, *Nat. Commun.* **2015**, *6*, 8831.
[40] X. Gong, M. Tong, Y. Xia, W. Cai, J. S. Moon, Y. Cao, G. Yu, C.-L. Shieh, B. Nilsson, A. J. Heeger, *Science* **2009**, *325*, 1665.
[41] S. Liu, Z. Wei, Y. Cao, L. Gan, Z. Wang, W. Xu, X. Guo, D. Zhu, *Chem. Sci.* **2011**, *2*, 796.
[42] P. Hu, L. Wang, M. Yoon, J. Zhang, W. Feng, X. Wang, Z. Wen, J. C. Idrobo, Y. Miyamoto, D. B. Geohegan, *Nano Lett.* **2013**, *13*, 1649.
[43] J. Wojtas, J. Mikolajczyk, Z. Bielecki, *Sensors* **2013**, *13*, 7570.

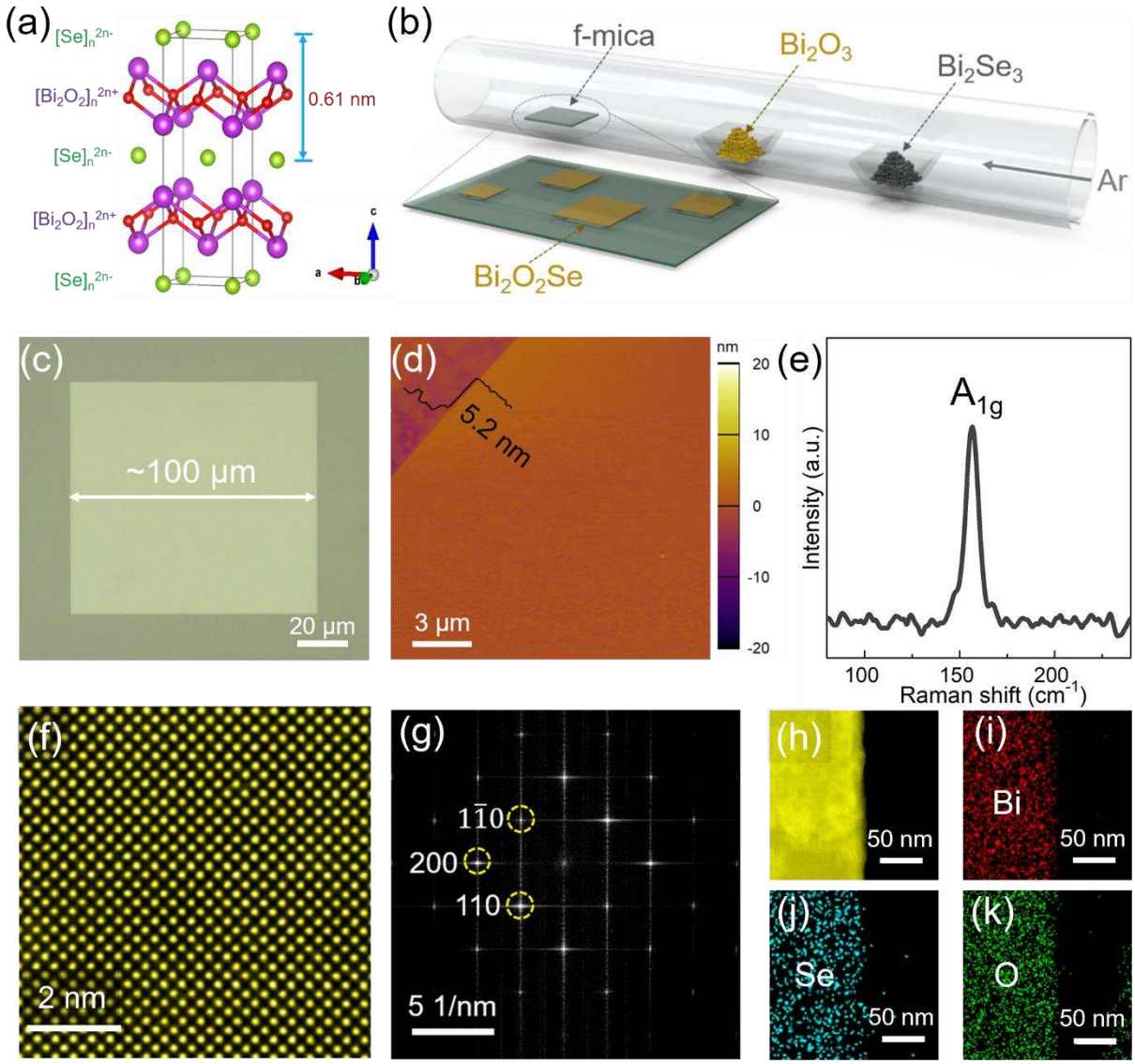

Figure 1. CVD Synthesis and characterization of Bi_2O_2Se. (a) Crystal structure of Bi_2O_2Se. (b) Schematic of the CVD setup for the synthesis of Bi_2O_2Se. (c) Optical image of square Bi_2O_2Se on f-mica. The size is around 100 μm. (d) AFM topography of the as-grown Bi_2O_2Se. The thickness is around 5.2 nm, which is consistent with an eight-layer sample. (e) Raman spectrum of Bi_2O_2Se with the characteristic A_{1g} peak at 159.1 cm^{-1}. (f) The atomic-resolution ADF-STEM image of Bi_2O_2Se shows tetragonally arranged atoms. (g) FFT pattern of (f). Squarely arranged spots indicate the crystal space group of I4/mmm. (h-k) Low magnification ADF-STEM image (h) and EDS mappings of elements Bi (i), Se (j) and O (k) at region (h), showing uniform distribution of the three elements.

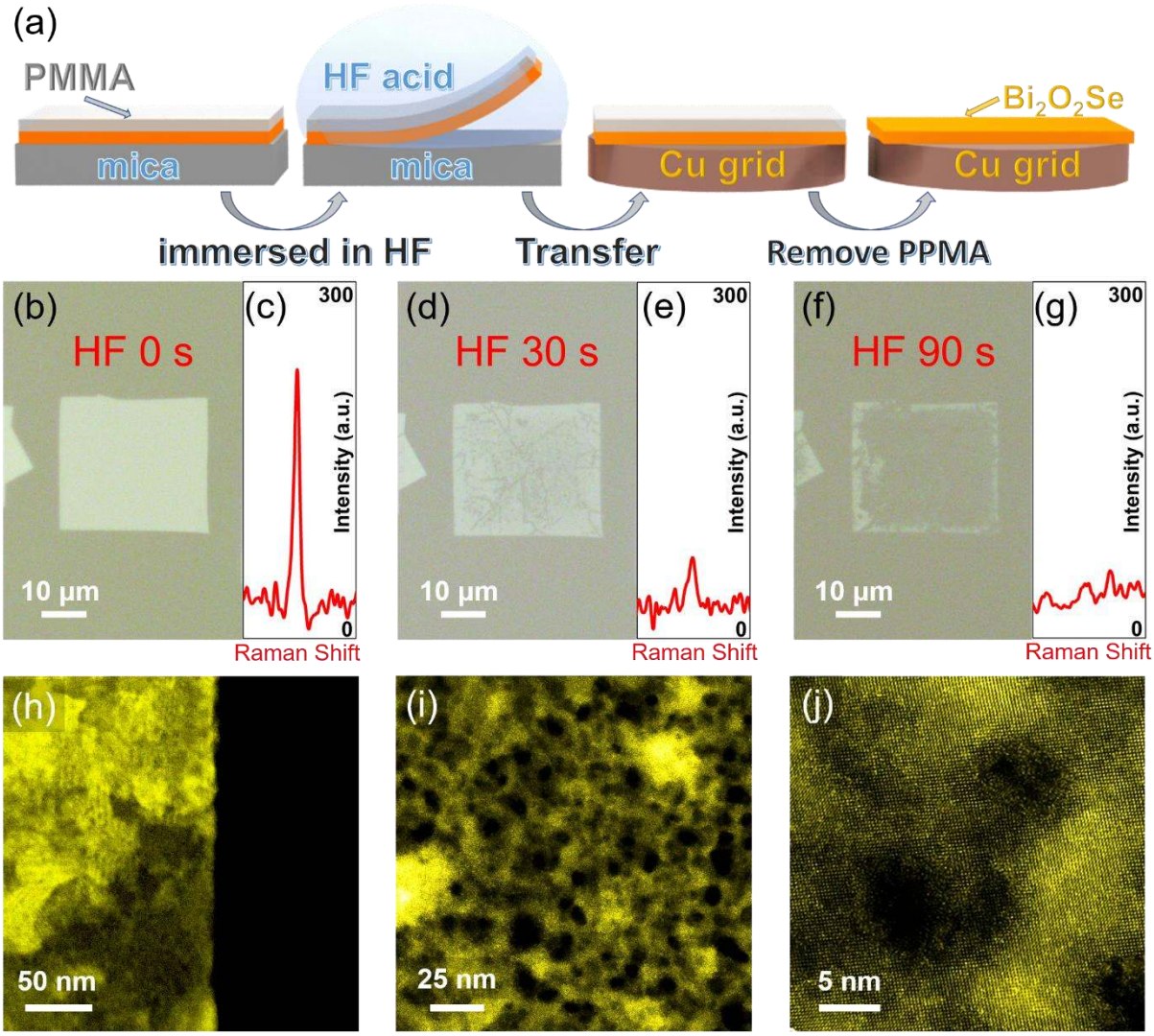

Figure 2. Etching effect of HF acid on Bi_2O_2Se. (a) Schematic of normal transfer process using HF acid. (b-g) Changes of optical images and Raman spectra of Bi_2O_2Se with the HF treatment for different times. (b-c) Initial state. (d-e) Partial etching and disappearance of the Raman peak at 30 s. (f-g) Almost full etching and nearly disappearance of the Raman peak at 90 s. (h) Low magnification ADF-STEM image shows non-uniform contrast, which indicates the inhomogeneous surface etched by HF acid. (i) Nanopores in Bi_2O_2Se after the transfer using HF acid and a magnified image (j).

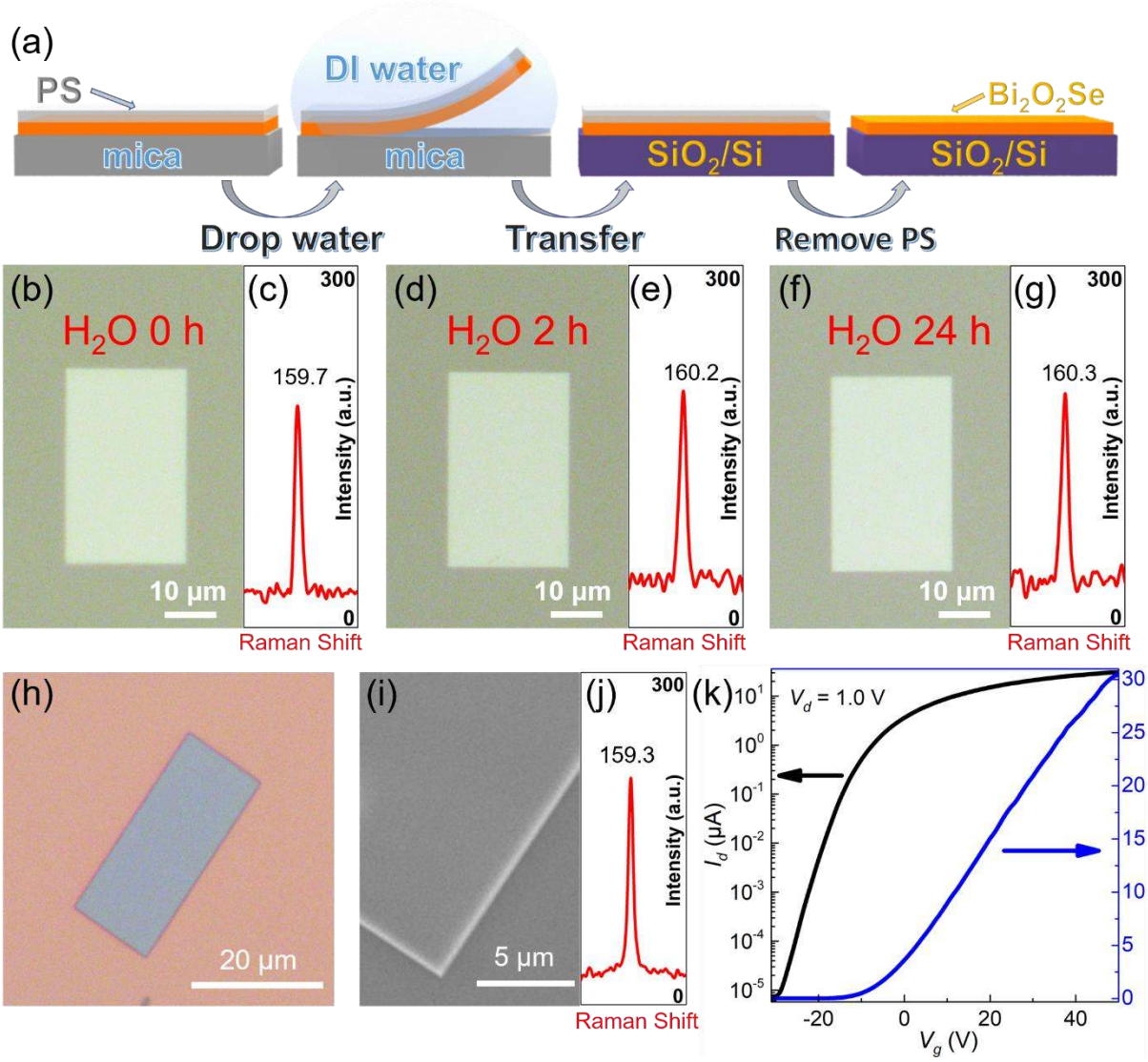

Figure 3. PS-assisted transfer and characterization of Bi_2O_2Se. (a) Schematic of PS-assisted transfer process. (b-g) Changes of optical images and Raman spectra of Bi_2O_2Se with the DI water treatment at different times. (b-c) Initial state. (d-g) No obvious changes could be observed after the DI water treatment with 2 h and 24 h, which indicates good stability of Bi_2O_2Se during this process. (h) Optical image and (i) SEM image shows the uniform contrast, indicating the success of the developed non-corrosive method. (j) Raman spectrum of the as-transferred Bi_2O_2Se on Si substrate. (k) FET I_d-V_g curve of the as-transferred Bi_2O_2Se. The mobility is calculated to be about 107 $cm^2V^{-1}s^{-1}$.

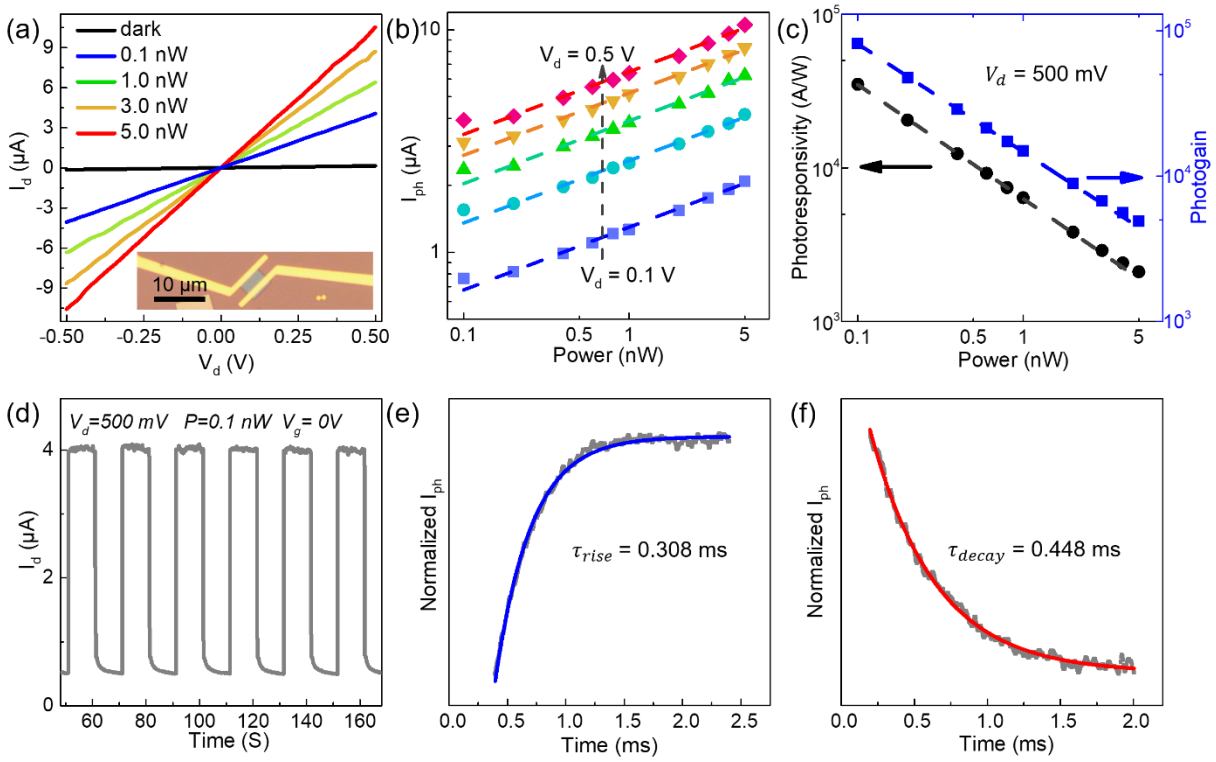

Figure 4. Photoresponse performances of the as-transferred Bi_2O_2Se. (a) FET I_d-V_d curves of the as-transferred Bi_2O_2Se under different light powers. Inset: the optical image of the device. (b-c) The light power dependence of (b) photocurrent (I_{ph}) as a function of bias, and (c) the photoresponsivity (R) and photogain (G). The maximum R and G are 3.5×10^4 AW^{-1} and 8.0×10^4, respectively. (d) The on/off test of photocurrent under the power of 0.1 nW and the bias of 0.5 V. The photoresponsivity is as high as 3.5×10^4 AW^{-1}. (e-f) The exponential fitting of the dynamic response of photocurrent for the rise (e) and decay (f). The deduced rise (τ_{rise}) and decay (τ_{decay}) time constants are about 0.308 and 0.448 ms.

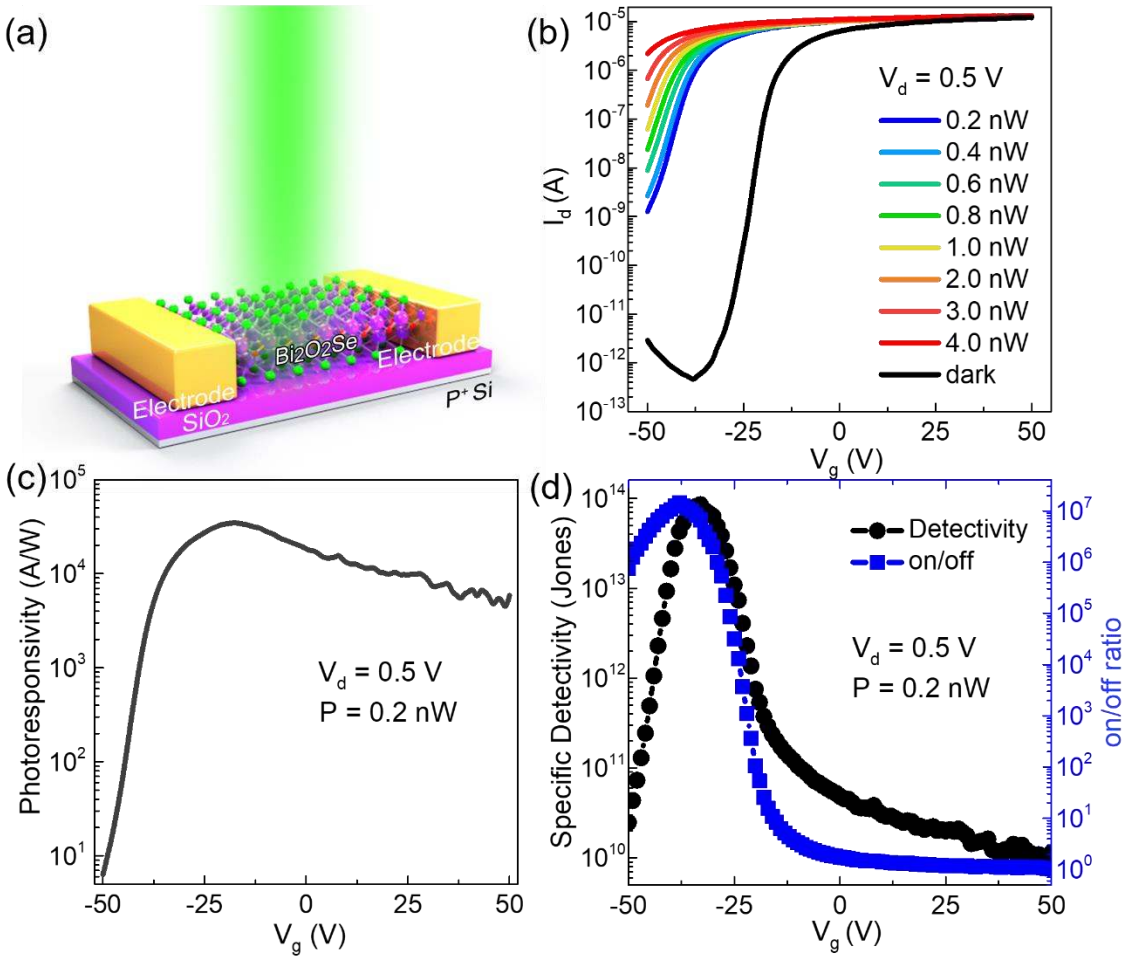

Figure 5. Gate-tunable photoresponse of the as-transferred Bi_2O_2Se. (a) Schematic of the Bi_2O_2Se phototransistor on a Si substrate, which provides the convenience of back gating. (b) FET I_d-V_g curve of the as-transferred Bi_2O_2Se under different light powers. The dark current could be reduced to several pA. (c) The gate voltage dependence of the photoresponsivity, ranging from 10 to 3.6×10^4 AW^{-1}. (d) The gate voltage dependence of the specific detectivity and on/off ratio. The maximum on/off ratio and detectivity are ~10^7 and 9×10^{13} Jones, respectively.

Table 1. Comparison of phototransistor performance based on the as-transferred Bi_2O_2Se with other 2D semiconductors prepared by CVD or mechanical exfoliation (ME) methods.

Materials	Fabrication method	Responsivity/V_d ($AW^{-1}V^{-1}$)	Detectivity (Jones)	Rise time (ms)	Ref.
MoS_2	CVD	0.057	1×10^{10}	0.07	29
ReS_2	CVD	1208	4.44×10^{10}	2	30
SnS_2	CVD	0.0044	1×10^{9}	0.005	31
$SnSe_2$	CVD	337	1×10^{10}	14.5	13
InSe	ME	15.7	1×10^{11}	50	34
In_2Se_3	ME	79	1×10^{10}	18	33
GaTe	ME	55	1×10^{12}	48	32
Bi_2O_2Se	CVD	70000	9×10^{13}	0.308	This work

The table of contents: Ultrasensitive Bi_2O_2Se phototransistor is demonstrated by utilizing a unique method to transfer CVD-grown Bi_2O_2Se from mica onto silicon substrate. Compared with devices on mica, while the photodetectors on silicon maintain high photoresponsivity, high photoconductive gain, fast response rate, and at the same time, the dark current was much lowered, which yields ultrahigh on/off ratio and specific detectivity.

Keywords: two-dimensional materials, field-effect transistors, bismuth oxyselenide, phototransistor, silicon substrate.

Ultrasensitive Two-dimensional Bi_2O_2Se Phototransistors on Silicon Substrates

ToC figure

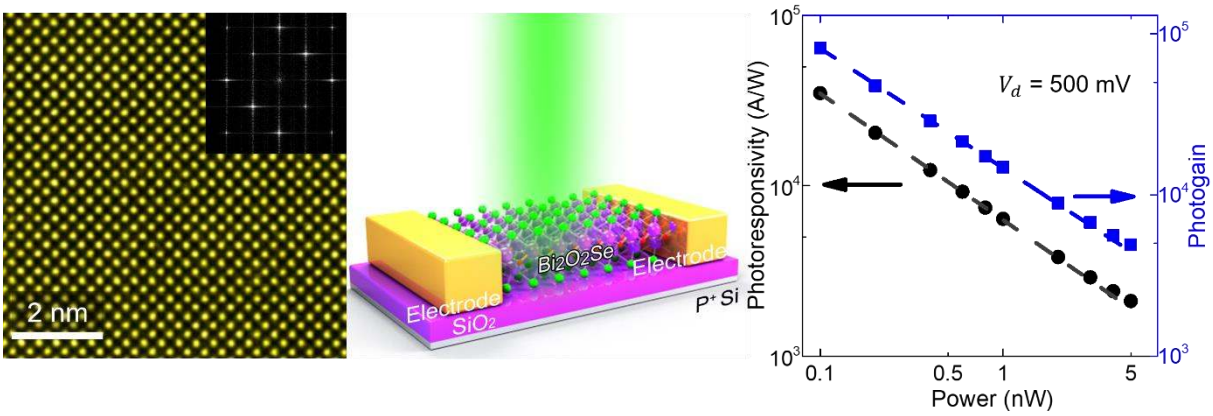

Supporting Information

Ultrasensitive Two-dimensional Bi_2O_2Se Phototransistors on Silicon Substrates

Qundong Fu, Chao Zhu, Xiaoxu Zhao, Xingli Wang, Apoorva Chaturvedi, Chao Zhu, Xiaowei Wang, Qingsheng Zeng, Jiadong Zhou, Fucai Liu, Beng Kang Tay, Hua Zhang, Stephen John Pennycook*, and Zheng Liu**

Qundong Fu, Chao Zhu, Dr. Apoorva Chaturvedi, Dr. Chao Zhu, Dr. Xiaowei Wang, Dr. Qingsheng Zeng, Dr. Jiadong Zhou, Dr. Fucai Liu, Prof. Hua Zhang, Dr. Zheng Liu
School of Materials Science and Engineering, Nanyang Technological University, Singapore 639798, Singapore
E-mail: z.liu@ntu.edu.sg.
Dr. Xiaoxu Zhao, Prof. Stephen Pennycook
National University of Singapore, Department of Materials Science and Engineering, 9 Engineering Drive 1, Singapore 117575, Singapore
E-mail: steve.pennycook@nus.edu.sg.
Dr. Xingli Wang, Dr. Zheng Liu, Prof. Beng Kang Tay
CINTRA CNRS/NTU/THALES, UMI 3288, Research Techno Plaza, Singapore 637553, Singapore
Dr. Fucai Liu
School of Optoelectronic Science and Engineering, University of Electronic Science and Technology of China, Chengdu, 610054, China.
E-mail: fucailiu@uestc.eu.cn.

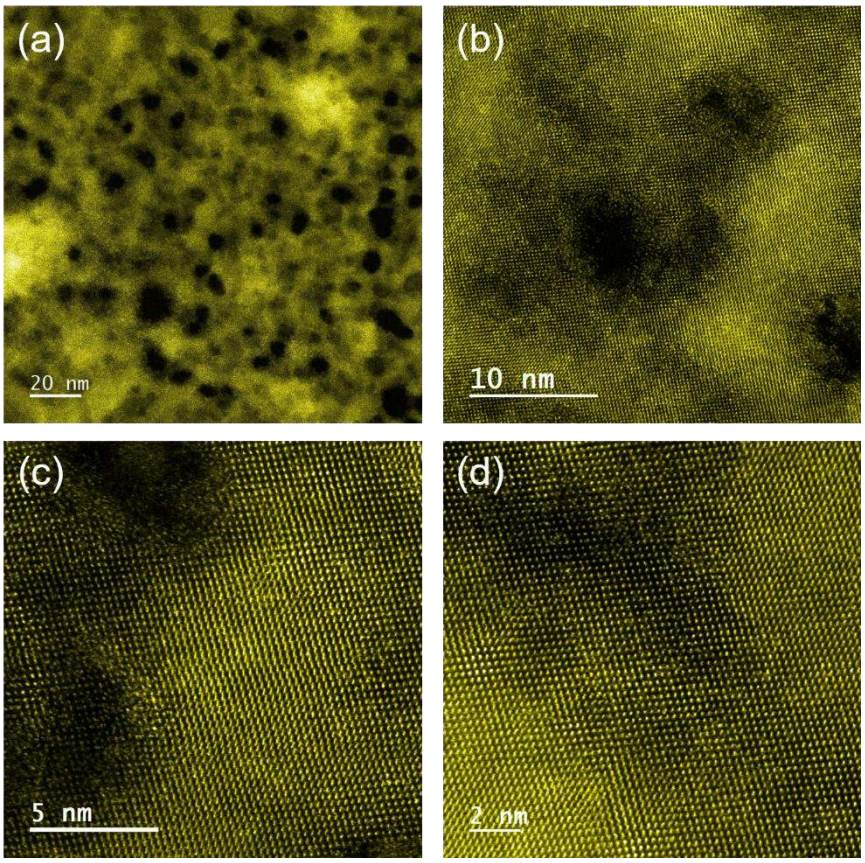

Figure S1. HF etching effect. (a-d) The evidence that nanopores exist in ADF-STEM images under different magnifications proves that Bi_2O_2Se has been etched by HF acid during the transfer process.

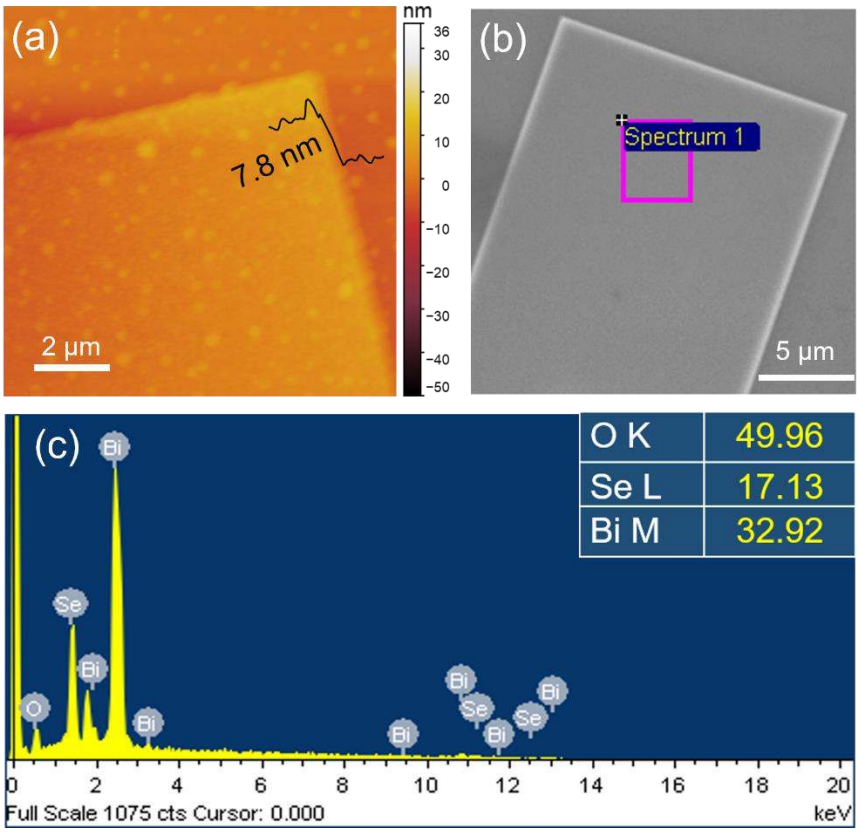

Figure S2. AFM and SEM EDS of the as-transferred Bi_2O_2Se. (a) AFM topography of the as-transferred Bi_2O_2Se. The thickness obtained from the height profile is about 7.8 nm. (b) SEM image shows the uniform contrast of the sample surface. (c) EDS of the as-transferred Bi_2O_2Se, marked with pink square in (b). The ratio of Bi to Se is about 1.93, which shows a good chemical stoichiometry.

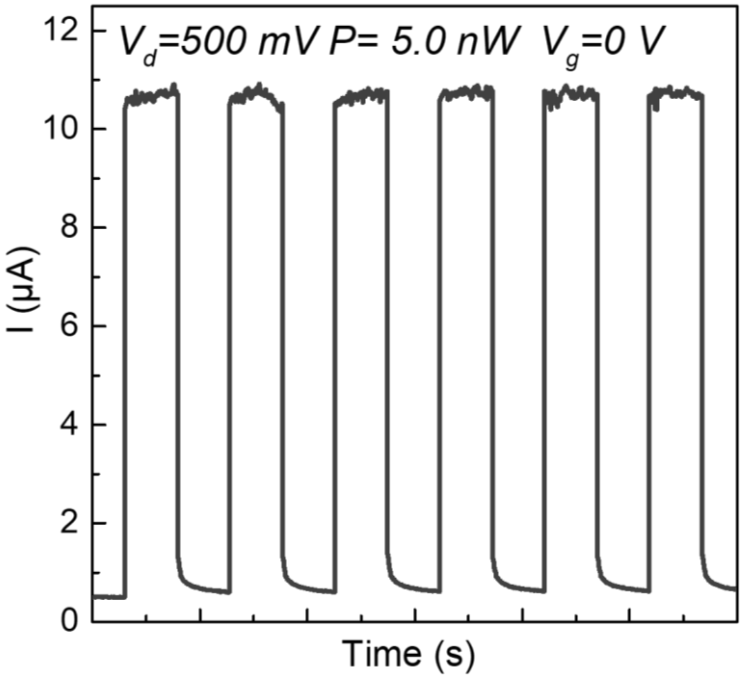

Figure S3. The largest photocurrent (10.7 μA) obtained without gate voltage.

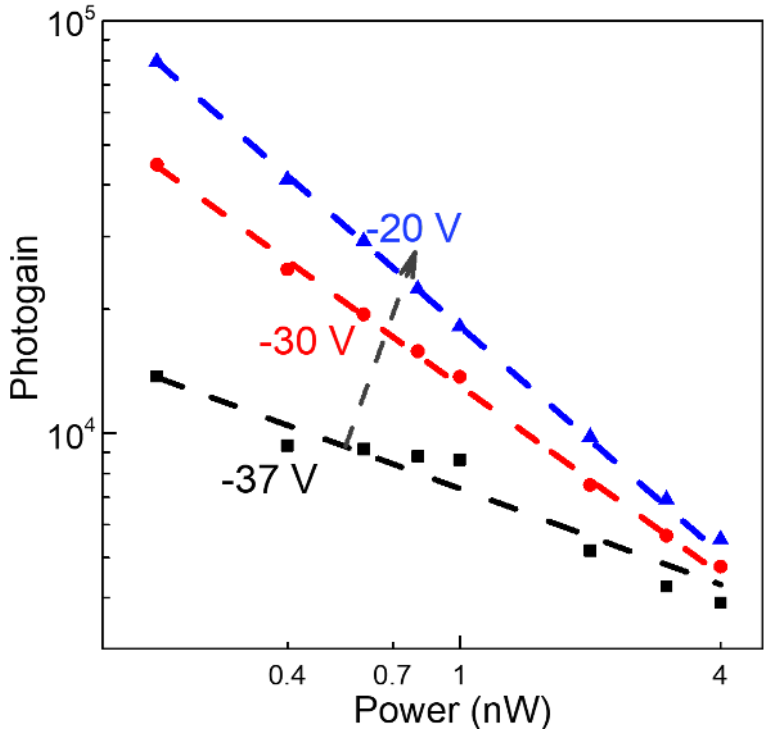

Figure S4. The power dependence of photoconductive gain at three gate voltages.